Published in final edited form as:

Magn Reson Imaging. 2015 June ; 33(5): 525–530. doi:10.1016/j.mri.2015.02.006.

Prostate Cancer Discrimination in the Peripheral Zone With a Reduced Field-of-View T_2-mapping MRI Sequence

Fernando I. Yamauchi, MD[1,2], **Tobias Penzkofer, MD**[1,3], **Andriy Fedorov, PhD**[1], **Fiona M. Fennessy, MD, PhD**[4], **Renxin Chu, PhD**[1], **Stephan E. Maier, MD, PhD**[1,5], **Clare M.C. Tempany, MD**[1], **Robert V. Mulkern, PhD**[1,6], and **Lawrence P. Panych, PhD**[1]

[1]Department of Radiology, Brigham and Women's Hospital, Harvard Medical School, Boston, MA

[2]Instituto de Radiologia do Hospital das Clínicas da Faculdade de Medicina da Universidade de São Paulo. São Paulo, SP, Brazil

[3]Department of Radiology, Charité Universitätsmedizin Berlin, Berlin, Germany

[4]Department of Imaging, Dana-Farber Cancer Institute, Harvard Medical School, Boston, MA

[5]Department of Radiology, Sahlgrenska University Hospital, Gothenburg University, Gothenburg, Sweden

[6]Department of Radiology, Children's Hospital Boston, Harvard Medical School, Boston, MA

Abstract

Objectives—To evaluate the performance of T_2 mapping in discriminating prostate cancer from normal prostate tissue in the peripheral zone using a practical reduced field-of-view MRI sequence requiring less than 3 minutes of scan time.

Materials and Methods—Thirty-six patients with biopsy-proven peripheral zone prostate cancer without prior treatment underwent routine multiparametric MRI at 3.0T with an endorectal coil. An Inner-Volume Carr-Purcell-Meiboom-Gill imaging sequence that required 2.8 minutes to obtain data for quantitative T_2 mapping covering the entire prostate gland was added to the routine multiparametric protocol. Suspected cancer (SC) and suspected healthy (SH) tissue in the peripheral zone were identified in consensus by three radiologists and were correlated with available biopsy results. Differences in mean T_2 values in SC and SH ROIs were tested for significance using unpaired Student's two-tailed t test. The area under the receiver operating characteristic curve was used to assess the optimal threshold T_2 value for cancer discrimination.

Results—ROI analyses revealed significantly ($p<0.0001$) shorter T_2 values in SC (85.4 ± 12.3 ms) compared to SH (169.6 ± 38.7 ms). An estimated T_2 threshold of 99 ms yielded a sensitivity of 92% and a specificity of 97% for prostate cancer discrimination.

Corresponding Author and Reprint Information: Lawrence P. Panych, 75 Francis Street, Boston, MA 02115, Tel: 617-278-0615, Fax: 617-264-5275, panych@bwh.harvard.edu.

Conclusions—Quantitative values derived from this clinically practical T_2-mapping sequence allow high precision discrimination between healthy and cancerous peripheral zone in the prostate.

Keywords

quantitative MRI; T_2 mapping; prostate MRI; prostate cancer

1. Introduction

Prostate cancer is the leading cause of non-cutaneous cancer diagnosed among men in the US and is the second most common cause of cancer death, exceeded only by lung cancer [1]. Despite extensive research in the field, many uncertainties remain about this disease, including screening strategies, non-invasive assessment of aggressiveness and treatment options for different grades of cancer. In this setting, prostate MRI has been the focus of extensive research to help improve accuracy in not only ruling out significant disease, but also characterizing and grading tumors, vital information for disease management and treatment stratification.

MRI has been successfully used to stage prostate cancer since the late-1980s, primarily with T_2-weighted (T2W) and T_1-weighted (T1W) imaging sequences. There has been continual improvement in hardware, including the incorporation of endorectal coils, and in software development of pulse sequences suitable for diffusion weighted imaging (DWI), spectroscopy and dynamic contrast enhanced (DCE) studies [2]. Given recent interest in focal therapies and active surveillance as viable options for prostate cancer treatment and the addition of multiparametric imaging capabilities with the technical advances, there is a shifting emphasis towards non-invasive detection, localization and characterization of the disease in addition to staging with MRI.

It is widely appreciated that peripheral zone prostate cancer often has low signal on T_2 weighted images [3], making T2W imaging a key, if subjective, assessment for cancer detection. Quantitative measurement of T_2 and the generation of T_2 maps for prostate cancer detection has been previously reported [4–9] but is not routinely used clinically nor is as ubiquitous as mapping of the apparent diffusion coefficient (ADC) value, a quantitative technique used routinely in prostate cancer staging and detection, in conjunction with visual impressions from the raw diffusion weighted images [2].

The decrease of signal on T2W images within the peripheral zone that accompanies focal cancer indicates a shortening of the T_2-decay and so it seems somewhat surprising that the use of quantitative T_2 values to discriminate prostate cancer from normal peripheral zone has not been exploited to a greater degree. This may in part be attributed to the prolonged scan times associated with acquiring multiple echo time (TE) data sets required for T_2 evaluation. Our goal in this work was to evaluate the performance of T_2 mapping for discriminating areas of suspected prostate cancer from suspected normal glandular tissue in the peripheral zone when using a practical Inner-Volume Carr-Purcell-Meiboom-Gill (IV-CPMG) imaging sequence.

2. Materials and Methods

2.1. Patient population

Patients with newly diagnosed biopsy-proven adenocarcinoma of the prostate without prior treatment undergo routine multiparametric 3 Tesla MRI at our institution for the purposes of treatment staging or active surveillance. Between November 2012 and February 2013, 45 consecutive of these patients (median age 60 years; range 50–72 years) had an additional sequence for T_2 mapping added to their MRI protocol. The study was performed under an Institutional Review Board-approved protocol and informed consent was obtained prior to MRI and signed by each patient and a study coordinator.

Of the 45 patients who underwent the additional imaging, four were later excluded from the study either because it was found that there was an absence of a suspicious lesion in the peripheral zone or there was a suspicious lesion but it was in the central gland or anterior fibro-muscular stroma (e.g. based on clinical T_2-weighted and diffusion-weighted images). Five other patients were excluded because there was significant motion artifact on the T_2 mapping sequence used for the study.

Image data from 36 patients (out of the initial 45 patients that had T_2 mapping) were included in the final study. Of the patients whose data was included, nine had low-risk, 21 had intermediate-risk and six had high-risk prostate cancer (D'Amico's risk criteria [10]). At the time of enrollment, the mean serum prostate-specific antigen (PSA) level was 8.5 ng/mL (range 3.6–21.8 ng/mL). Indications for MRI were mainly for staging (n=28), but also included active surveillance (n=8). The time of biopsy prior to the MRI ranged from 7 to 551 days with a median and standard deviation of 51 and 127 days respectively. Several patients had multiple biopsies.

2.2. Imaging sequences and parameters

All patients included in this study underwent multiparametric MRI under a standard protocol that is used at our institution for the assessment of intra and extra-glandular prostate disease. Imaging was performed using a 3T Signa HDxt scanner (General Electric Medical Systems) operating under software version 15.0. The MRI protocol, which included the use of an air-filled endorectal coil (Medrad Inc. Indianola, PA, USA) combined with an eight-element flexible torso phased-array coil, has been described previously [2]. Briefly, T_1-weighted spoiled gradient echo (SPGR) imaging in the axial plane, T_2-weighted Fast Spin Echo (FSE) imaging in all three planes, as well as axial DWI and DCE imaging were performed.

The unique component of this study was the inclusion of an IV-CPMG imaging sequence for T_2 mapping. The manufacturer's clinical FSE sequence includes a CPMG option whereby individual spin echoes in the echo train can be used to obtain images with different TE's in a single acquisition. This sequence was modified in-house to obtain the IV-CPMG sequence used in the study. In the modified sequence, the excitation and refocusing pulses were tilted with respect to each other, as discussed by Rangwala and Zhou [11] and shown schematically in Fig. 1. This tilting has the effect not only of selectively exciting spins in the slice direction but also of restricting the volume of spins excited along the phase encode direction through selective refocusing. The images in Fig. 1 demonstrate the ability of the

sequence to select a reduced field-of-view without significant aliasing in the phase-encode direction.

The preferred image orientation for prostate T2W prostate imaging is axial and the R-L direction is normally selected as the phase-encoding direction to avoid having motion artifacts from the rectal wall obscure the prostate. The same axial orientation and selection of phase and frequency directions was adopted for T_2 mapping. Without restricting the selected volume in the phase direction, a FOV of over 300 mm would be required. However, the IV-CPMG sequence allowed us to greatly reduce the phase FOV (and, thus, the number of phase encoding steps) while avoiding aliasing artifact.

For a tilt angle of φ (assuming it is less than about 40°) the restricted volume in the phase direction equals two times the slice thickness multiplied by tangent(90°-φ). In this study, we used tilts of approximately 4° to select an 85 mm section in the phase direction for a slice thickness of 3 mm. The FOV in the frequency direction was 140 mm and the selected matrix size was 192 × 160 in frequency and phase directions respectively. With the phase-encoding FOV set to 62% and with the half-Fourier option added, the actual number of phase encodes was reduced to approximately 50, which included a slight oversampling for the half-FT phase correction. Thus, even with a relatively long TR, the scan times were only 2.8 minutes compared to almost 9 minutes scans that would be required for a full-FOV, full-Fourier acquisition. A total of 8 spin echoes per slice were acquired at TE's from 18 to 144 ms at intervals of 18 ms. With a TR of 3300 ms, 20 slices could be acquired in one acquisition, allowing for full gland coverage in the axial plane (slice thickness: 3 mm, slice gap: 1 mm). The resultant in-plane resolution was approximately 1 × 1.5 mm^2.

An undesired side effect due to tilting the spatially selective excitation with respect to refocusing is that the flip angle of the refocusing pulses becomes dependent on the position of the spins not just along the slice direction, as in slice selective CPMG imaging, but also along the phase-encode direction. That is, in standard slice selective CPMG imaging, the variability of the refocusing flip angles within the slice-selection profiles results in contributions from stimulated echoes and a departure of the resulting signal decays with echo time from pure T_2 decays. A noticeable feature of this effect is a surprisingly lower signal on first echo images and calculated T_2 values longer than expected due to T_1 contributions. Thus, the estimated T_2 is more aptly referred to as the 'apparent' T_2. In the IV-CPMG sequence used in this study, we expected such effects to be exacerbated due to the additional flip angle variation along the phase-encode direction. This is demonstrated in Fig. 2, which shows T_2 estimates using the standard full-FOV CPMG sequence compared with the T_2 estimates in a doped water phantom (T_2 ~60ms) obtained using the IV-CPMG sequence. Near the center of the reduced FOV the two methods are in close agreement in terms of the estimated T_2, however, near the edges the difference increases significantly. In the studies reported here, the gland was positioned at the center of the reduced FOV to minimize such effects though they certainly contribute to inaccuracies in T_2 values, which are understood to be "apparent" T_2 values.

2.3. Image Analysis

Two radiologists (FIY and TP), aware of all clinical information (indication for the exam, clinical stage, PSA values and biopsy results), reviewed multiparametric MRI data sets (including DWI and DCE images) and identified one suspected cancer (SC) lesion per patient in consensus. When consensus was not reached, a third senior radiologist (FMF) was consulted. Regions-of-Interest (ROIs) corresponding to SC were then mapped to the T_2 maps generated from the IV-CPMG sequence. When consensus was reached, another ROI corresponding to suspected healthy (SH) tissue in the peripheral zone was used for comparative analysis. This ROI was placed in a region of homogeneously high signal intensity, containing as much normal appearing glandular tissue as possible. For three of the patients, no consensus was reached on an acceptable SH ROI, thus, the analysis included results from 36 SC ROIs but only 33 SH ROIs.

The detailed prostate pathology report for each patient was available to the radiologists at the time of ROI selection. All information available from the pathology report was used to confirm that the suspected cancer ROIs were placed in the location of the pathology-proven cancer. While correlation with whole-mount pathology would be preferable, this was not feasible for the study as not all patients went to prostatectomy (only 9 of 36).

Quantitative T_2 maps were generated from the IV-CPMG data by assuming a monoexponential T_2 decay. The first echo was not used in the analysis because it is typically found to have less signal intensity than the 2^{nd} echo, as noted previously with the use of slice selective CPMG sequences in the prostate [7]. Furthermore, signals from later echoes were discarded prior to fitting if the signal was within 3 standard deviations of baseline noise values as measured in air containing-ROIs placed in the rectum. The T_2-mapping analysis was performed using a custom processing routine implemented within 3D Slicer (http://www.slicer.org), an open source image guided therapy and image analysis platform [12]. Differences in mean T_2 values in SC and SH ROIs were tested for significance using an unpaired Student's two-tailed *t*-test with statistical significance assumed at $p<0.05$. Normality of the T_2 data was confirmed via the Shapiro-Wilks test. The area under the receiver operating characteristic curve (AUC) was used to assess the optimal threshold T_2 value for cancer discrimination. Statistical analyses were performed using MedCalc for Windows, version 12.5 (MedCalc Software, Ostend, Belgium).

3. Results

A single slice image with corresponding results of T_2 analysis from the IV-CPMG acquisition of one of the patients is shown in Fig. 3. The image for the fourth echo with a TE of 72 ms is shown (Fig. 3a) along with ROIs in the peripheral zone corresponding to suspected cancer and suspected healthy tissue. Figure 3b shows signal values on a logarithmic scale along with the least-square fits for the multi-echo data. Note that the data from the first echo was not used when fitting data to estimate the apparent T_2 for reasons discussed above. The T_2 map estimated from the IV-CPMG data is also shown (Fig. 3c).

In all 36 eligible patients, a single ROI for the suspected index cancer lesion was identified. Suspected healthy peripheral zone was identified in only 33 of the patients. In the remaining

three, no consensus could be reached for SH, as no area of homogeneous high T2W-signal region could be identified. The 36 ROIs identified as SC had an average size of 203 pixels (range 4–1124), whereas the 33 ROIs identified as SH had an average size of 72 pixels (range 24–240). Whenever possible, the same slice was used to identify both SC and SH ROIs (n=11). When not in the same slice, ROIs from SC and SH were one (n=4), two (n=9), four (n=7) and six (n=2) slices apart from each other.

The average T_2 value (85.4 ± 12.3 ms) extracted from ROIs that were identified as SC was significantly shorter ($p<0.0001$) than the mean T_2 value (169.6 ± 38.7 ms) extracted from ROIs identified as SH (see Fig. 4).

In the ROC analysis, differences in mean T_2 values showed a discriminatory performance of AUC=0.985 ($p<0.0001$) (Fig. 5). Further analysis of the data showed that, by choosing a threshold of 99ms, a sensitivity of 91.7% and a specificity of 97.0% could be achieved.

4. Discussion

MRI-based detection, localization and characterization of lesions are extremely important in achieving efficacy with focal therapies as treatment alternatives to radical prostatectomy and radiation therapy [13,14] and several studies have shown the benefits of multiparametric prostate MRI in this context [15–17]. Quantitative imaging and analysis may have a special role to play considering the strong evidence of an inverse relationship between ADC values and Gleason grade [18–24] and the apparent correlation between pharmacokinetic parameters obtained in DCE studies of prostate cancer. A key advantage of quantitative imaging is that it provides greater objectivity in image analysis. It may also improve sensitivity and specificity in detecting and characterizing lesions when compared to qualitative-based approaches.

Although there has been a shift towards more quantitative analyses in the prostate imaging community, with an emphasis on ADC values [25] and pharmacokinetic parameters, quantitative T_2 analyses has remained largely within the realm of research [2]. It is perhaps somewhat surprising that quantitative T_2 analysis is not more prevalent considering that conventional T_2-weighted imaging is very much in the front-line for visualization of prostate anatomy and identification of suspected regions of cancer. Signal intensity at a single TE is an amalgam of several effects, including not only the T_2 value, but also receiver coil sensitivities, B1 inhomogeneities, and T_1 and proton density effects. Thus, T_2 mapping in addition to standard T2W imaging should be advantageous as it is insensitive to some of these confounding effects.

There are significant technical challenges in obtaining quantitative T_2 maps in the clinical setting. First, the gold standard T_2 mapping approach of performing multiple single spin-echo acquisitions with a range of TE settings requires excessive scan times. More practical approaches have included the use of separate fast spin echo (FSE) acquisitions with different effective TEs. However, each scan still requires several minutes to cover the gland with adequate spatial resolution [5,6,26]. Wei et al exploited an accelerated imaging approach [9], however, the total acquisition time for T_2 mapping was still almost 6 minutes and the whole prostate was not covered. Roebuck et al [7] utilized direct CPMG imaging, which

provides multiple TEs in a single acquisition, but the 12-minute scan time was not very practical for routine clinical use. In addition, the use of multiple slice-selective refocusing pulses introduces stimulated echo effects into T_2-decay curves [27–29].

We sought to determine if a rapid and clinically practical CPMG technique could provide T_2 values that, although probably not "accurate" due to stimulated-echo effects, could still provide clinically significant discrimination between prostate cancer and healthy peripheral zone tissue. The values so obtained and analyzed in this work appear quite useful for cancer discrimination with, for example, a threshold T_2 of 99 ms yielding a sensitivity of 92% and a specificity of 97% for discriminating cancer from healthy tissue. The actual T_2 values obtained in this work are consistent with those previously found in prostate cancer and healthy peripheral zone using slower T_2 mapping methods [5–7].

Potential additions to the approach used here could significantly improve the accuracy of the T_2 estimates. For example, with some modification to the RF excitation profiles [30] it is possible to obtain much more uniform flip angle distributions over the selected volume to minimize spatially-dependent variation in T_2 estimates. Also, combining the IV-CPMG sequence with a reconstruction approach such as that proposed by Ben-Eliezer et al [31] could be used to correct for the stimulated echo effects and provide more accurate T_2 estimates. Other methods for selecting the reduced FOV might also be considered, such as those methods discussed in [32].

A recent prostate MR guideline stated the importance of quantitative measurements and structured reporting [33], as they can help not only to improve inter-observer agreement but also to develop computer-aided detection systems. There is a potential benefit of incorporating quantitative T_2 values into computer-aided detection systems rather than visual interpretation of T2W alone, as has been shown in a recent report that utilized T_2-weighted signal intensity histogram (skewness) [34]. Whether the use of quantitative T_2 measurements can improve the specificity and/or sensitivity of prostate cancer detection over qualitative analysis still remains to be answered but appears, in light of this work and others, to be quite promising.

As a note of caution, it should be stated that there are disease entities associated with shorter T_2 values (and lower T2W signal) in the peripheral zone other than prostatic adenocarcinoma. Post-prostate biopsy hemorrhage can leave foci of methaemoglobin scattered in the gland and lower the T2W signal. This complication can be avoided if one is able to rule out hemorrhage by assessing the same location on T1W images (as was done in this study) or by simply allowing sufficient time between biopsy and imaging. Further, benign conditions such as acute and chronic prostatitis can also lead to low T2W-signal areas within the PZ. In most cases, these can be distinguished from cancer by morphology, since prostatitis has a "band-like" or linear shape and cancer is typically a round focal mass.

Our study has some limitations. First, only a relatively small set of patients was examined. Second, we recognize that the pathological correlation of the suspected cancer lesion on MRI with the biopsy results has limitations and is not as accurate as radical prostatectomy. This is a persistent limitation of all biopsy correlation studies. Third, we assumed a normal

appearing peripheral zone without histopathologic correlation. However, we did make efforts to select the normal ROIs in homogeneous regions of high signal in the PZ on T2W images, in an attempt to minimize potential confounders such as prostatitis that are known to reduce peripheral zone T_2 signal.

In conclusion, the IV-CPMG imaging sequence allowed for reasonably rapid estimates of quantitative T_2 values. This quantification could increase the effectiveness of multiparametric MRI in the detection and staging of prostate cancer without adding significantly to the time required for image acquisition.

Acknowledgments

Sources of Support: NIH: R01CA111288, R01CA109246, R01CA160902, R33CA110092, U01CA151261, P01CA067165, P41RR019703, P41EB015898.

References

1. Jemal A, Siegel R, Xu J, Ward E. Cancer statistics, 2010. CA Cancer J Clin. 2010; 60(5):277–300. [PubMed: 20610543]
2. Hegde JV, Mulkern RV, Panych LP, et al. Multiparametric MRI of prostate cancer: An update on state-of-the-art techniques and their performance in detecting and localizing prostate cancer. J Magn Reson Imaging. 2013; 37(5):1035–1054. [PubMed: 23606141]
3. Yu KK, Hricak H. Imaging prostate cancer. Radiol Clin North Am. 2000; 38(1):59–85. viii. [PubMed: 10664667]
4. Engelbrecht MR, Huisman HJ, Laheij RJ, et al. Discrimination of prostate cancer from normal peripheral zone and central gland tissue by using dynamic contrast-enhanced MR imaging. Radiology. 2003; 229(1):248–254. [PubMed: 12944607]
5. Gibbs P, Tozer DJ, Liney GP, Turnbull LW. Comparison of quantitative T2 mapping and diffusion-weighted imaging in the normal and pathologic prostate. Magn Reson Med. 2001; 46(6):1054–1058. [PubMed: 11746568]
6. Liney GP, Knowles AJ, Manton DJ, Turnbull LW, Blackband SJ, Horsman A. Comparison of conventional single echo and multi-echo sequences with a fast spin-echo sequence for quantitative T2 mapping: application to the prostate. Journal of magnetic resonance imaging : J Magn Reson Imaging. 1996; 6(4):603–607.
7. Roebuck JR, Haker SJ, Mitsouras D, Rybicki FJ, Tempany CM, Mulkern RV. Carr-Purcell-Meiboom-Gill imaging of prostate cancer: quantitative T2 values for cancer discrimination. Magn Reson Imaging. 2009; 27(4):497–502. [PubMed: 18823731]
8. Wang L, Mazaheri Y, Zhang J, Ishill NM, Kuroiwa K, Hricak H. Assessment of biologic aggressiveness of prostate cancer: correlation of MR signal intensity with Gleason grade after radical prostatectomy. Radiology. 2008; 246(1):168–176. [PubMed: 18024440]
9. Liu W, Turkbey B, Senegas J, Remmele S, Xu S, Kruecker J, Bernardo M, Wood BJ, Pinto PA, Choyke PL. Accelerated T_2 mapping for characterization of prostate cancer. Magn Reson Med. 2011; 65:1400–1406. [PubMed: 21394778]
10. D'Amico AV, Moul J, Carroll PR, Sun L, Lubeck D, Chen MH. Cancer-specific mortality after surgery or radiation for patients with clinically localized prostate cancer managed during the prostate-specific antigen era. J Clin Oncol. 2003; 21(11):2163–2172. [PubMed: 12775742]
11. Rangwala N, Zhou XJ. Reduction of fast spin echo cusp artifact using a slice-tilting gradient. Magn Reson Med. 2010; 64(1):220–228. [PubMed: 20572152]
12. Fedorov A, Beichel R, Kalpathy-Cramer J, et al. 3D Slicer as an image computing platform for the Quantitative Imaging Network. Magn Reson Imaging. 2012; 30(9):1323–1341. [PubMed: 22770690]

13. Barnes AS, Haker SJ, Mulkern RV, So M, D'Amico AV, Tempany CM. Magnetic resonance spectroscopy-guided transperineal prostate biopsy and brachytherapy for recurrent prostate cancer. Urology. 2005; 66(6):1319. [PubMed: 16360468]
14. Poissonnier L, Chapelon JY, Rouviere O, et al. Control of prostate cancer by transrectal HIFU in 227 patients. Eur Urol. 2007; 51(2):381–387. [PubMed: 16857310]
15. Delongchamps NB, Rouanne M, Flam T, et al. Multiparametric magnetic resonance imaging for the detection and localization of prostate cancer: combination of T2-weighted, dynamic contrast-enhanced and diffusion-weighted imaging. BJU Int. 2011; 107(9):1411–1418. [PubMed: 21044250]
16. Haider MA, van der Kwast TH, Tanguay J, et al. Combined T2-weighted and diffusion-weighted MRI for localization of prostate cancer. AJR Am J Roentgenol. 2007; 189(2):323–328. [PubMed: 17646457]
17. Turkbey B, Mani H, Shah V, et al. Multiparametric 3T prostate magnetic resonance imaging to detect cancer: histopathological correlation using prostatectomy specimens processed in customized magnetic resonance imaging based molds. J Urol. 2011; 186(5):1818–1824. [PubMed: 21944089]
18. deSouza NM, Riches SF, Vanas NJ, et al. Diffusion-weighted magnetic resonance imaging: a potential non-invasive marker of tumour aggressiveness in localized prostate cancer. Clin Radiol. 2008; 63(7):774–782. [PubMed: 18555035]
19. Hambrock T, Hoeks C, Hulsbergen-van de Kaa C, et al. Prospective assessment of prostate cancer aggressiveness using 3-T diffusion-weighted magnetic resonance imaging-guided biopsies versus a systematic 10-core transrectal ultrasound prostate biopsy cohort. Eur Urol. 2012; 61(1):177–184. [PubMed: 21924545]
20. Hambrock T, Somford DM, Huisman HJ, et al. Relationship between apparent diffusion coefficients at 3. 0-T MR imaging and Gleason grade in peripheral zone prostate cancer. Radiology. 2011; 259(2):453–461. [PubMed: 21502392]
21. Oto A, Yang C, Kayhan A, et al. Diffusion-weighted and dynamic contrast-enhanced MRI of prostate cancer: correlation of quantitative MR parameters with Gleason score and tumor angiogenesis. AJR Am J Roentgenol. 2011; 197(6):1382–1390. [PubMed: 22109293]
22. Turkbey B, Shah VP, Pang Y, et al. Is apparent diffusion coefficient associated with clinical risk scores for prostate cancers that are visible on 3-T MR images? Radiology. 2011; 258(2):488–495. [PubMed: 21177390]
23. Van As N, Charles-Edwards E, Jackson A, et al. Correlation of diffusion-weighted MRI with whole mount radical prostatectomy specimens. Br J Radiol. 2008; 81(966):456–462. [PubMed: 18487387]
24. Vargas HA, Akin O, Franiel T, et al. Diffusion-weighted endorectal MR imaging at 3 T for prostate cancer: tumor detection and assessment of aggressiveness. Radiology. 2011; 259(3):775–784. [PubMed: 21436085]
25. Mazzoni LN, Lucarini S, Chiti S, Busoni S, Gori C, Menchi I. Diffusion-weighted signal models in healthy and cancerous peripheral prostate tissues: Comparison of outcomes obtained at different b-values. J Magn Reson Imaging. 2014; 39(3):512–518. [PubMed: 23723087]
26. Chan I, Wells W 3rd, Mulkern RV, et al. Detection of prostate cancer by integration of line-scan diffusion, T2-mapping and T2-weighted magnetic resonance imaging; a multichannel statistical classifier. Phys. 2003; 30(9):2390–2398.
27. Poon CS, Henkelman RM. 180o refocusing pulses which are insensitive to static and radiofrequency field inhomogeneity. J Magn Reson Imaging. 1992; 99:45–55.
28. Prasloski T, Madler B, Xiang QS, MacKay A, Jones C. Applications of stimulated echo correction to multicomponent T2 analysis. Magn Reson Med. 2012; 67(6):1803–1814. [PubMed: 22012743]
29. Fennessy FM, Fedorov A, Gupta SN, Schmidt EJ, Tempany CM, Mulkern RV. Practical considerations in T1 mapping of prostate for dynamic contrast enhancement pharmacokinetic analyses. Magn Reson Imaging. 2012; 30(9):1224–1233. [PubMed: 22898681]
30. Maier SE. Slab Scan Diffusion imaging. Magn Reson Med. 2001; 46(6):1136–1143. [PubMed: 11746580]

31. Ben-Eliezer N, Sodickson DK, Block KT. Rapid and accurate T2 mapping from multi-spin-echo data using Bloch-simulation-based reconstruction. Magn Reson Med. 2014 Epub ahead of print.
32. Wargo CJ, Moore J, Gore JC. A comparison and evaluation of reduced-FOV methods for multi-slice 7T imaging. Magn Reson Imag. 2013; 31:1349–1359.
33. Barentsz JO, Richenberg J, Clements R, et al. ESUR prostate MR guidelines 2012. Eur Radiol. 2012; 22(4):746–757. [PubMed: 22322308]
34. Peng Y, Jiang Y, Yang C, et al. Quantitative Analysis of Multiparametric Prostate MR Images: Differentiation between Prostate Cancer and Normal Tissue and Correlation with Gleason Score--A Computer-aided Diagnosis Development Study. Radiology. 2013; 267(3):787–796. [PubMed: 23392430]

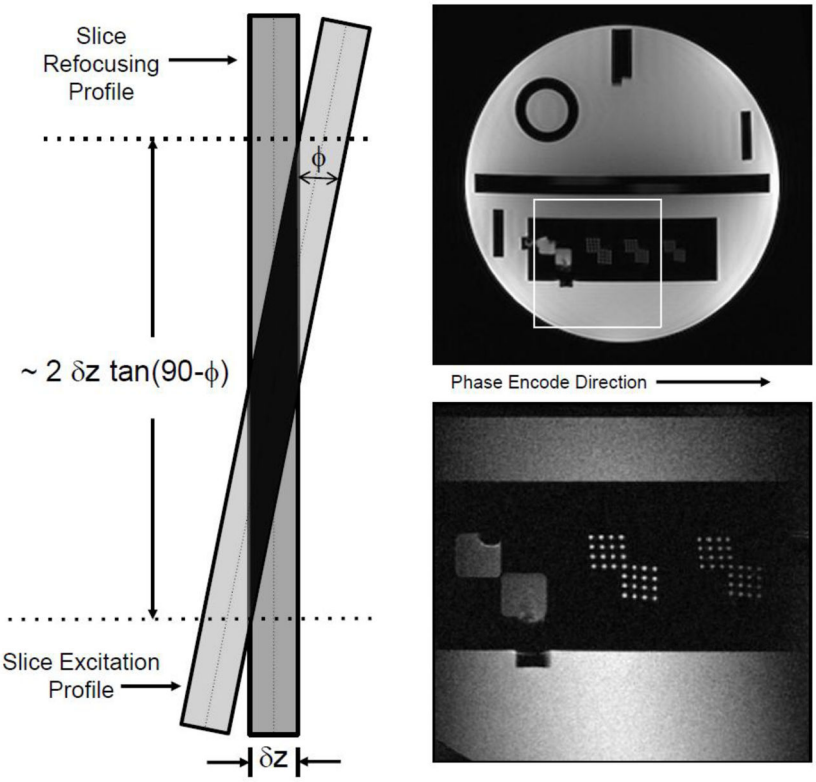

Figure 1.

Left: The schematic shows the spatial selection scheme used in the IV-CPMG sequence whereby the slice selection profile is tilted with respect to the refocusing profile. This has the effect of restricting the imaging volume in a second (phase-encoding) direction. Right Top: Full FOV phantom image. Right-Bottom: A reduced FOV image (1/3 FOV in both phase and frequency directions) of the same phantom. The image was produced using IV-CPMG, which is an in-house-modified clinical fast-spin-echo sequence. The FSE sequence has an option whereby all spin echoes in the echo train are phase encoded identically allowing for T_2-mapping.

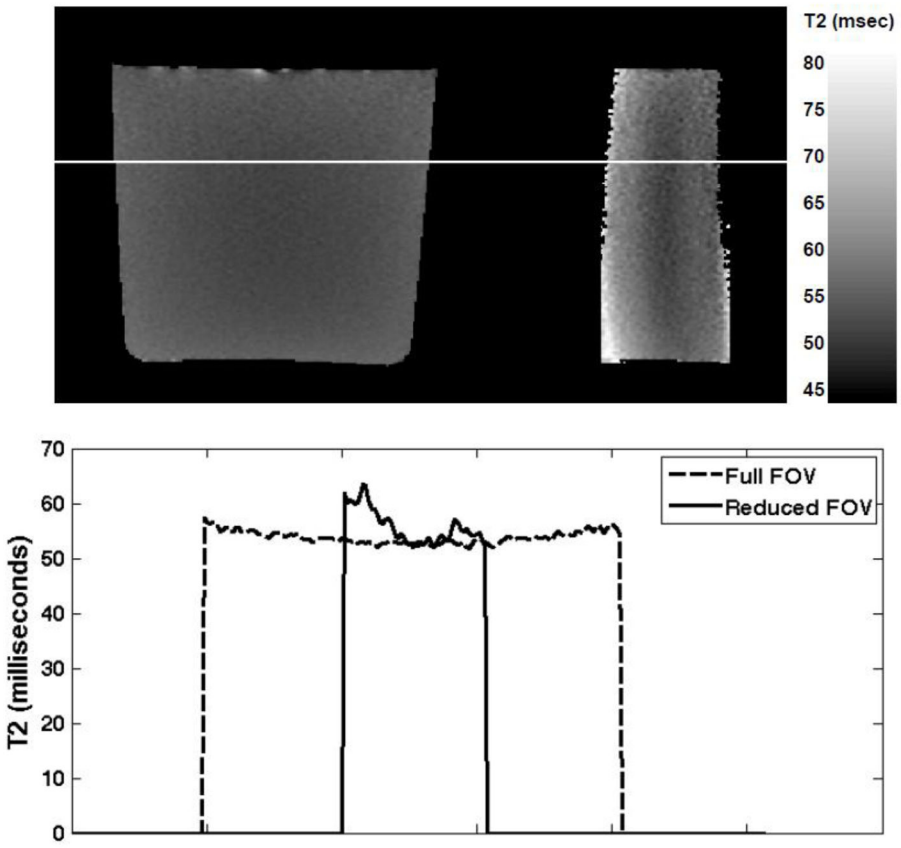

Figure 2.

Top: T_2 maps for one slice obtained using a doped water phantom (0.5 mM $MnCl_2$ with relaxivity of 35 s^{-1}/mM giving a T_2 of ~60ms). The image on the left shows the T_2 map for the full FOV obtained using a standard CPMG sequence. The image shows the T_2 map for the same slice using the IV-CPMG sequence. Bottom: Plots of the estimated T_2 values for one row in the images above. The location of the plotted data is indicated by the white line in the images.

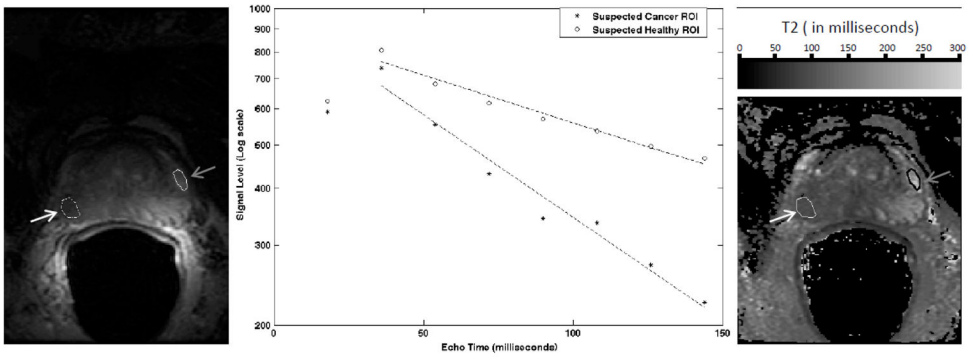

Figure 3.

T_2 mapping analysis. (a) A single slice image from the IV-CPMG acquisition of one patient. The image is for the fourth echo (TE = milliseconds). ROIs for regions in the peripheral zone of suspected cancer (white arrow) and suspected healthy (gray arrow) are overlaid. (b) The signal values and fits for all 8 echoes are shown for the suspected cancer ('*') and suspected healthy ('o') regions. The data from the first echo was not used when fitting data to estimate T_2 (see text for discussion). The mean T_2's for the ROIs are 96 (cancer) and 208 milliseconds (healthy). (c) The T_2 map estimated from the IV-CPMG data is displayed along with the ROIs.

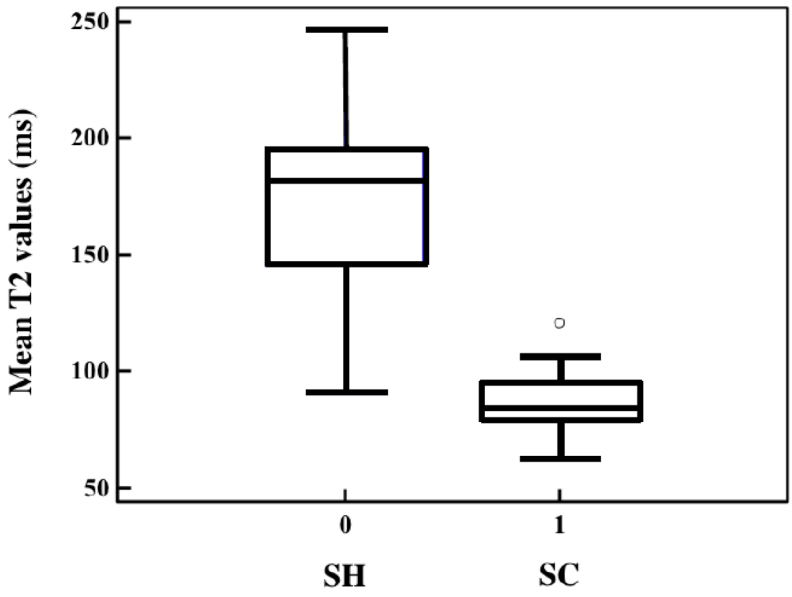

Figure 4.

Boxplots of mean T_2 values in SH and SC regions. The mean T_2 value (85.4 ± 12.3 ms) in SC regions was significantly ($p<0.0001$) shorter than the T_2 (169.6 ± 38.7 ms) in SH regions.

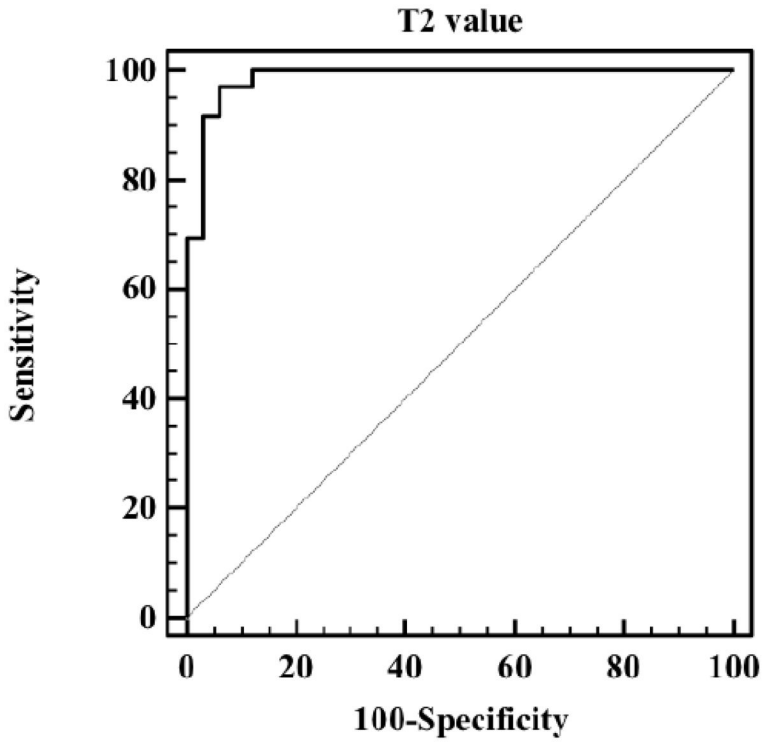

Figure 5.

The ROC curve obtained by setting thresholds on T_2 measures for the selected SC and SH regions. A 92% sensitivity and 97% specificity is achieved for a T_2 threshold of 99 ms (AUC=0.985).